Time-Reversal Massive Multipath Effect: A Single-Antenna "Massive MIMO" Solution

Yi Han, Yan Chen, Beibei Wang, and K. J. Ray Liu

Origin Wireless Inc., College Park, MD 20742, USA

ECE Dept., University of Maryland, College Park, MD 20742, USA

Email: {yhan1990, yan, bebewang and kjrliu}@umd.edu

Abstract

The explosion of mobile data traffic calls for new efficient 5G technologies beyond what current 4G LTE can provide. Massive MIMO, which has shown the great potential in improving the achievable rate with a very large number of antennas, becomes a popular candidate. However, several critical challenges in designing the analog front-end and coordinating the large-scale antenna array have to be carefully addressed before the massive MIMO can be actually adopted. Therefore, a natural question to ask is: does there exist a good alternative that can achieve similar system performance to massive MIMO with a simpler design? In this paper, we show that by using time-reversal approach, with a sufficiently large bandwidth, one can harvest massive multipath naturally existing in the environment to form high number of virtual antennas to achieve the desired massive MIMO effect with a single antenna. We answer the above question by analyzing the time-reversal massive multipath effect (TRMME) and the achievable rate with different signature waveforms. We also derive the corresponding asymptotic achievable rate under a massive multipath setting. Experiment result based on real channel measurements shows the approach to realize the massive multipaths in practical environment. Moreover, based on our experiment with real indoor measurement, even with only a single antenna, the time-reversal wideband system can achieve comparable performance as the massive MIMO system in terms of expected achievable rate.

Index Terms

Massive MIMO, time-reversal (TR), time-reversal division multiple access (TRDMA), time-reversal massive multipath effect (TRMME), expected achievable rate

I. INTRODUCTION

While the past few decades has witnessed the monumental success of mobile and wireless access to the Internet, the proliferation of new mobile communication devices, such as smartphones and tablets, has in turn led to an exponential growth in network traffic. According to the most recent Cisco Visual Networking Index (VNI) annual report [1], the global mobile data traffic grew 69% and the number of mobile devices increased almost half a billion (497 million) in 2014. It is also predicted in the report that the global mobile data traffic will increase nearly tenfold between 2014 and 2019. The demand for supporting the fast-growing consumer data rates urges the wireless service providers and researchers to seek a new efficient radio access technology, which is the so-called 5G technology, beyond what current 4G LTE can provide. Besides ultra-densification and mmWave, massive multiple-input multiple-output (MIMO) is one of "big three" 5G technology [2], which can offer multi-fold benefits such as enormous enhancement in spectral efficiency and power efficiency [3] and simple transmit/receiver structures due to the quasi-orthogonal nature [4]. These benefits make massive MIMO one of the five disruptive technology directions for 5G communication [5].

Even though the benefits of massive MIMO seem very promising, several critical challenges must first be addressed before it can be implemented in practice. First of all, a challenging task is the analog front-end design [6], for example, each tiny antenna need its own power amplifier and analog-to-digital convertor (ADC). Moreover, the antenna correlation and mutual coupling due to the increasing number of antennas has to be carefully addressed as well [7] [8]. The researchers in Lund University built a 100-antenna MIMO testbed, and the size is $0.8 \times 1.2 \times 1$ m with 300kg weight and 2.5kW average power consumption [9]. Considering the challenges of massive MIMO in hardware design and coordinating the large scale antenna array, a natural question to ask is: does there exist a good alternative that can achieve similar system performance to massive MIMO with a simpler implementation? The answer is yes and the time-reversal (TR) technology is potentially a counterpart of massive MIMO in 5G communications.

The straightforward approach to realize the massive MIMO effect is through utilizing an excessive amount of physical antennas as the current massive MIMO systems. On the other hand, it is well known that radio signals will experience many multipaths due to the reflection from various scatters, especially in indoor environment. TR's focusing effect is in essence a

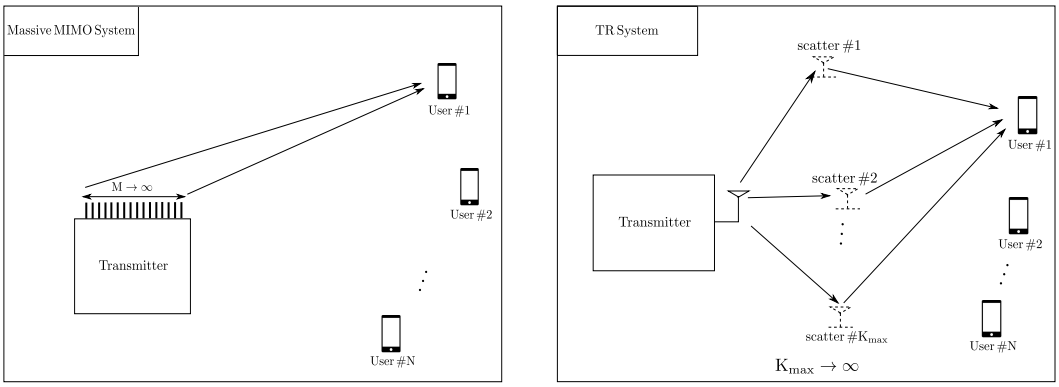

(a) An illustration of massive MIMO system

(b) An illustration of TR system

Fig. 1: Comparison between massive MIMO system and TR system

spatial-temporal resonance effect that brings all the multipaths to arrive at a particular location at a specific moment. Such a phenomenon will allow us to utilize the naturally existing multipaths as virtual antennas to be an alternative approach to realize "massive MIMO" effect even with a single antenna. As shown in Fig. 1, TR inherently treats the multipaths in the environment as virtual antennas, similar to MIMO that uses multiple antennas for better spatial multiplexing.

In order to harvest the multipaths, the transmit power and bandwidth can be utilized. More specifically, the maximum number of observable multipaths given by an environment increases with the transmit power. Once the power is fixed, the maximum number of observable multipaths is also fixed. In addition, more multipaths can be resolved with the increase of bandwidth because of the better time resolution. Based on the real indoor ultra-wide-band (UWB) channel measurement (both LOS and NLOS) in [10] and [11], around 60-80 independent multipaths can be revealed with a sufficiently large bandwidth. Later in Section VI, we will discuss about how to realize the massive multipath in practical indoor environment.

TR technology is a promising candidate for future communication, but it requires wide bandwidth to achieve good time resolution. First, as indicated by Moore's Law, the more powerful analog-to-digital-converter (ADC) and digital signal processor (DSP) make the wideband signal processing cost down dramatically [12] [13]. Moreover, researchers and engineers are currently searching for new available wide band and re-allocating bandwidth for 5G technology [2]. For TR technology, it may use the spectrum of ultra-wide-band (UWB) or mmWave band. Based on

the existing study at high frequencies, there still exists a large amount of multipaths, which is essential for TR communication. For example, based on the building penetration and reflection measurements of 28GHZ in NYC [14], the RF energy is mostly retained within buildings due to low attenuation and high reflection through indoor materials. Moreover, the delay spread for indoor 60GHz channels ranges between 30ns and 70ns [15], which indicates a multipath-rich environment. Furthermore, compared with increasing the spectral efficiency, it becomes more and more important to reduce complexity, total energy consumption and offer other benefits for 5G communication given the potential wide bandwidth.

By exploiting the massive number of virtual antennas, TR system can achieve superior focusing effect in spatial-temporal domain, resulting in similar performance as promised by massive MIMO. Moreover, the implementation complexity of TR system is much lower since it utilizes the environment as the virtual antenna array and computing resource. Specifically, in this paper, we consider a Time-Reversal Division Multiple Access (TRDMA) downlink communication system [16] to demonstrate the TR massive multipath effect (TRMME). Since advanced signature waveforms may be needed to suppress the ISI and IUI, we analyze the achievable rate of the TR system under different signature waveforms, i.e., the basic TR, zero-forcing (ZF) and minimum mean square error (MMSE) signature waveforms. We further derive the asymptotic achievable rate performance as the number of observable multipaths grows to infinity. Later, we discuss the approach to realize massive multipaths based on real-world channel measurements. Through the experiment with real indoor measurement, we show that a TR wideband system can achieve comparable achievable rate as the massive MIMO system with a single antenna and much lower implementation complexity.

The rest of this paper is organized as follows. We first discuss the existing related work in Section II. The system model is discussed in Section III. In Section IV, the notion of TRMME is introduced assuming that the TR system has the ability to reveal infinite multipaths. In Section V, the expected achievable rate of the TR system with basic TR, ZF and MMSE signatures are investigated. Moreover, the asymptotic achievable rate with the three different signatures is derived in a massive multipath setting. The approach to realize massive multipaths in practical environment is discussed based on the real-world channel measurements in Section VI. Finally, Section VII concludes the paper.

II. Related Work

The TR technology was first introduced to compensate the delay distortion on wired transmission lines by Bogert from Bell Labs in the fifties [17]. Then, it has been applied in various areas including ultrasonics [18], acoustical imaging [19], electromagnetic imaging [20], and underwater acoustic communication [21]. More recently, TR has drawn more and more attention from researchers in the wireless communications field [22] [23] [24]. Under a rich-scattering environment, a TR communication system is shown to have the spatial-temporal focusing effect and thus work as an ideal platform for green wireless communications [25] [26] in terms of lower power consumption and less radio pollution. A time-reversal division multiple access (TRDMA) scheme is proposed in [16] which utilizes the location-specific signature to separate different users' signal. The asymptotical spectral efficiency in UWB system with perfect channel state information (CSI) at the receiver is derived in [27]. In [28], the spectral efficiency in UWB system with different receiver structures is analyzed without considering the potential inter-symbol-interference (ISI) in the system. It is shown in [16] [29] that the TR communication system can be extended to multiple-antenna scenarios easily, and more advanced waveform design can be implemented to further suppress the ISI and inter-user-interference (IUI) to achieve higher data rate [30] [31]. Moreover, with a sufficiently large bandwidth, TR communication system can achieve comparable or even better performance than orthogonal frequency-division multiplexing (OFDM) communication systems in term of achievable rate [32]. The potential application of TR technology in the Internet of Things is discussed in [12].

A closely related technology to the TR is the code division multiple access (CDMA). While TR technology utilizes the location-specific signature waveforms to distinguish multiple users, CDMA employs spread-spectrum to allocate distinct orthogonal code to multiple users [33]. Compared with the TR technology, the data rate of CDMA is much lower. Moreover, since the bandwidth of spread spectrum signal in CDMA system is large, the transmit signal in both systems will experience the multipath propagation in the environment. While CDMA system utilizes the rake receiver to handle the multipaths, TR technology harvests the multipaths in the environment to perform the beamforming with the appropriate precoding at the transmitter, which results in much lower complexity at the receiver side.

Time-Reversal is neither a new terminology in MIMO technology as well. First of all, time-

reversal beamforming is well known as conjugate beamforming in MIMO systems when the system bandwidth is small [34]. Then, for wide-band, frequency-selective channel, OFDM can rigorously decompose the channel into parallel independent narrow-bandwidth sub-carriers, where TR precoding can be applied [35] [36]. Since OFDM has a loss in spectral and power efficiency owing to the insertion of cyclic prefix, TR can be also employed as the precoding scheme directly for the delay-spread channel [37] [38].

The focus of this paper is not on the combination of massive MIMO and TR technologies. Instead, we show that TR technology itself is a promising alternative approach to realize massive MIMO effect without using a large number of physical antennas. In the paper, we first derive the expected achievable rate with different signatures in TR system with considering the ISI in practical system. Then, the asymptotical performance of TR system is also analyzed. Together with the theoretic analysis of the expected achievable rate, the idea of realizing massive virtual antennas with a single physical one and the approach to resolve multipaths with the increase of bandwidth constitute the novelty of our paper.

III. System Model

In this paper, we consider a time-reversal downlink system where one transmitter simultaneously communicates with N distinct receivers through the TRDMA technique [16]. We assume that both the transmitter and receivers are equipped with one single antenna. However, the results can be easily extended to the multiple-antenna scenario.

A. Channel model

Suppose there are totally K_{max} independent multipaths from the transmitter to the j^{th} receiver, then the channel $h_j(t)$ can be written as

$$h_j(t) = \sum_{k=1}^{K_{max}} \tilde{h}_{j,k}\delta(t-\tau_k), \tag{1}$$

where $\tilde{h}_{j,k}$ and τ_k are the complex channel gain and path delay of the k^{th} path, respectively. Note that the delay spread of the channel is given by $\tau_C = \tau_{K_{max}}$.

Let W be the bandwidth of the TR system. Then, through Nyquist sampling, the discrete channel responses can obtained as

$$h_j[n] = \int_{n\tau_p-\tau_p}^{n\tau_p} p(n\tau_p-\tau)h_j(\tau)d\tau, \tag{2}$$

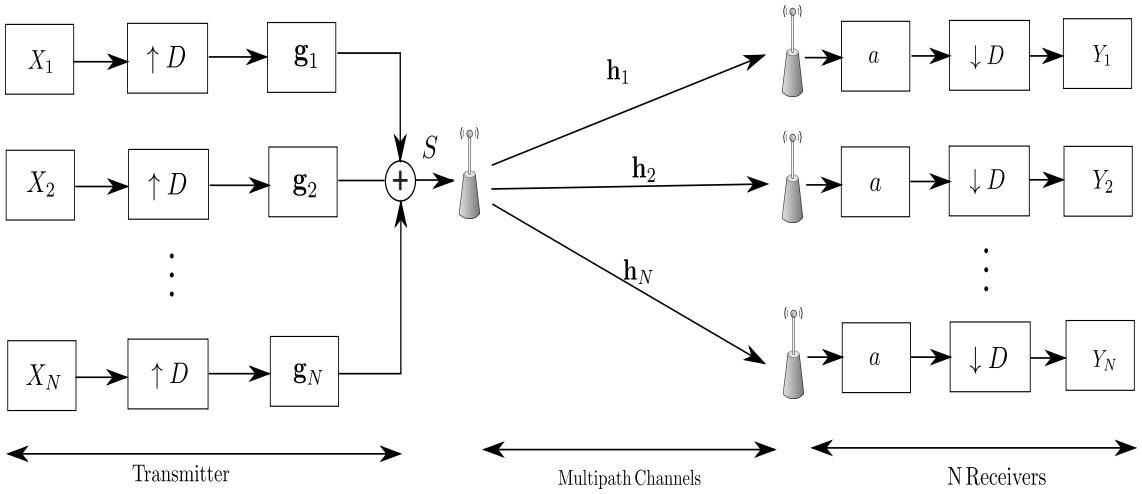

Fig. 2: TRDMA System

where $p(t)$ is the pulse with main lobe $\tau_p = 1/W$.

Through (2), a L-tap channel $\mathbf{h}_j = [h_j[1], h_j[2], ..., h_j[L]]^T$ with $L = round(\tau_C W)$ can be resolved for the link between the transmitter and the j^{th} receiver as follows

$$h_j[k] = \sum_{i=1}^{L} h_{j,i}\delta[k-i], \tag{3}$$

where $h_{j,i}$ is the complex channel gain of the i^{th} tap, and $h'_{j,i}s$ are independent for all $i \in [1, L]$ and $j \in [1, N]$.

Suppose that there are K non-zero elements in the L-tap channel $\mathbf{h}_j$. When the bandwidth W is small, all elements in $\mathbf{h}_j$ are generally non-zero, i.e., $K = L$. On the other hand, when W is sufficiently large, the side lobes of $p(t)$ becomes negligible and thus there are at most $K = K_{max} < L$ non-zero elements in $\mathbf{h}_j$. Let $\phi_{K_{max}}$ be the non-zero multipath set, which reflects the physical patterns of scatters distribution in the environment. Then, $h_j[k] = 0$ for $k \notin \phi_{K_{max}}$, and for $k \in \phi_{K_{max}}$, $h_j[k]$ is a complex random variable with zero mean and variance σ_k^2.

Prior to the TR-transmission, a pseudo random sequence is sent to the transmitter from the receiver, based on which the channel state information (CSI) $\mathbf{h}_j$ is estimated. By cross-correlating the received signal with the known pseudo random sequence, the power of CSI is boosted thus maintaining the good CSI quality. Due to the high speed system clock and the efficient Golay coorelator [39], the CSI estimation is obtained quickly in terms of time consumption. In addition,

based on the real measurement in [40], the CSI is quite stationary given only slightly changing of the environment, which indicates the channel need not to be re-probed very frequently and the overhead price of channel probing is very small.

B. TRDMA downlink communication

In the TR system, the transmitter simultaneously communicates with multiple receivers. Specifically, as shown in Fig. 2, the information to be transmitted to the j^{th} receiver, denoted as X_j, is first up-sampled by a backoff factor D to alleviate the interference, and then precoded by a signature waveform $\mathbf{g}_j$. Actually, the symbol rate is lower down by D to limit the ISI. Note that multiple designs of the signature waveform such as basic TR signature [25], zero-forcing (ZF) signature [41] and minimal mean square error (MMSE) signature [30] can be utilized, and the details will be discussed in the next section. After that, all signals to different receivers are mixed together as follows

$$S[k] = \sum_{i=1}^{N} \left(X_i^{[D]} * \mathbf{g}_i \right)[k]. \tag{4}$$

where

$$X_i^{[D]}[k] = \begin{cases} X_i[k/D], & \text{if } mod(k, D) = 0 \\ 0, & \text{otherwise} \end{cases} \tag{5}$$

The mixed signal is broadcast to all receivers through the rich-scatter environment. At the receiver side, the j^{th} receiver simply scales the received signal and down-samples it to obtain the estimated signal Y_j as follows

$$\begin{aligned} Y_j[k] =& (\mathbf{h}_j * \mathbf{g}_j)[L] X_j[k - \frac{L}{D}] \\ &+ \sum_{l=1, l \neq L/D}^{\frac{2L-1}{D}} (\mathbf{h}_j * \mathbf{g}_j)[Dl] X_j[k - l] \\ &+ \sum_{i=1, i \neq j}^{N} \sum_{l=1}^{\frac{2L-1}{D}} (\mathbf{h}_j * \mathbf{g}_i)[Dl] X_i[k - l] \\ &+ n_j[k]. \end{aligned} \tag{6}$$

Without loss of generality, we design the signature waveform so that $(\mathbf{h}_j * \mathbf{g}_j)$ has the resonating effect at time index L. Then the first term in (6) is the desired signal, the second term is the ISI, the third term is the IUI, and the last term is the noise.

The (6) can be re-written by replacing the convolution as inner product as follows

$$\begin{aligned} Y_j[k] = \mathbf{H}_j^{(\frac{L}{D})}\mathbf{g}_j X_j[k-\frac{L}{D}] + \sum_{l=1,l\neq L/D}^{(2L-1)/D} \mathbf{H}_j^{(l)}\mathbf{g}_j X_j[k-l] \\ + \sum_{l=1}^{(2L-1)/D} \mathbf{H}_j^{(l)} \left(\sum_{i=1,i\neq j}^{N} \mathbf{g}_i X_i[k-l] \right) + n_j[k], \end{aligned} \tag{7}$$

where $\mathbf{H}_j^{(m)}$ is the m^{th} row of the $(2L-1)/D \times L$ matrix $\mathbf{H}_j$ decimated by rows of Toeplitz matrix, which can be written as follows

$$\mathbf{H}_j = \begin{pmatrix} h_j[D] & h_j[D-1] & \cdots & h_j[1] & 0 & \cdots & \cdots & 0 \\ h_j[2D] & h_j[2D-1] & \cdots & \cdots & h_j[1] & 0 & \cdots & 0 \\ \vdots & \vdots & \ddots & \ddots & \ddots & \ddots & \ddots & \vdots \\ h_j[L] & h_j[L-1] & \cdots & \cdots & \cdots & \cdots & \cdots & h_j[1] \\ \vdots & \vdots & \ddots & \ddots & \ddots & \ddots & \ddots & \vdots \\ 0 & \cdots & 0 & h_j[L] & \cdots & \cdots & h_j[L-D+1] & h_j[L-2D] \\ 0 & \cdots & \cdots & 0 & h_j[L] & \cdots & h_j[L-D+1] & h_j[L-D] \end{pmatrix} \tag{8}$$

and thus $\mathbf{H}_j^{(\frac{L}{D})}$ is the time-reversal channel

$$\mathbf{H}_j^{(\frac{L}{D})} = [h_j(L)\, h_j(L-1) \cdots h_j(1)]. \tag{9}$$

C. Expected Achievable Rate for Individual User

Let P and P_n be the average transmitting power and noise power, respectively, and $(\cdot)^\dagger$ represent the conjugate transpose operator. According to (7) and the uplink-downlink duality [42] [43] [44], the achievable rate of the j^{th} receiver can be derived using its dual uplink format, where the uniform power allocation is assumed. Then we take an expectation of the downlink achievable rate as shown in (10). In the rest of the paper, we analyze the expected achievable rate of the TR system.

$$R_j = \frac{W}{D}\mathbb{E}\left[\log_2 \left(1 + \frac{\frac{P}{N}\mathbf{g}_j^\dagger \mathbf{H}_j^{(\frac{L}{D})\dagger}\mathbf{H}_j^{(\frac{L}{D})}\mathbf{g}_j}{\frac{P}{N}\mathbf{g}_j^\dagger \left(\mathbf{H}_j^\dagger \mathbf{H}_j - \mathbf{H}_j^{(\frac{L}{D})\dagger}\mathbf{H}_j^{(\frac{L}{D})} \right)\mathbf{g}_j + \frac{P}{N}\sum_{i=1,i\neq j}^{N} \mathbf{g}_j^\dagger \mathbf{H}_i^\dagger \mathbf{H}_i \mathbf{g}_j + P_n} \right) \right] \tag{10}$$

IV. TIME-REVERSAL MASSIVE MULTIPATH EFFECT

Similar to the quasi-orthogonal property in massive MIMO given an excessive amount of antennas [4], the multipath profile of different users in the TR system will also be orthogonalized given massive independent multipaths, which is called the TR Massive Multipath Effect (TRMME).

Time-Reversal Massive Multipath Effect (TRMME): Under the asymptotic setting where $K = K_{max} \to \infty$, $\mathbf{Q}\mathbf{Q}^\dagger$ converges to a diagonal matrix in distribution, and

$$\frac{[\mathbf{Q}\mathbf{Q}^\dagger]_{l_j,l_j}}{\|\mathbf{h}_j\|^2} \xrightarrow{d} 1, \tag{11}$$

where $\mathbf{Q} = [\mathbf{H}_1^T, \mathbf{H}_2^T, \cdots, \mathbf{H}_N^T]^T$.

Proof: In order to reveal all the observable multipaths, e.g., $K = K_{max}$, the bandwidth of the system W should be large enough so that $L/K_{max}^p \to c$ where $p > 2$. Notice that every element in $\mathbf{Q}\mathbf{Q}^\dagger$ is the sum of multiple independent variables, which converges to a Gaussian random variable in distribution in the asymptotical scenario based on the central limit theorem. Since Gaussian random variable is only determined by the first and second moment and obviously each element in $\mathbf{Q}\mathbf{Q}^\dagger$ has zero mean, we only need to prove the largest variance of off-diagonal element will converge to zero.

Based on the definition of $\mathbf{Q}$, we have

$$\mathbf{Q}\mathbf{Q}^\dagger = \begin{bmatrix} \mathbf{H}_1\mathbf{H}_1^\dagger & \mathbf{H}_1\mathbf{H}_2^\dagger & \cdots & \mathbf{H}_1\mathbf{H}_N^\dagger \\ \mathbf{H}_2\mathbf{H}_1^\dagger & \mathbf{H}_2\mathbf{H}_2^\dagger & \cdots & \mathbf{H}_2\mathbf{H}_N^\dagger \\ \vdots & \vdots & \ddots & \cdots \\ \mathbf{H}_N\mathbf{H}_1^\dagger & \mathbf{H}_N\mathbf{H}_2^\dagger & \cdots & \mathbf{H}_N\mathbf{H}_N^\dagger \end{bmatrix}. \tag{12}$$

With (12), we can directly obtain

$$\left[\mathbf{Q}\mathbf{Q}^\dagger\right]_{l_j,l_j} = \mathbf{H}_j^{(\frac{L}{D})}\mathbf{H}_j^{(\frac{L}{D})\dagger} = \|\mathbf{h}_j\|^2. \tag{13}$$

where $[\cdot]_{m,n}$ represents the element in the m^{th} row and the n^{th} column of the matrix.

Then, we prove that $\mathbf{Q}\mathbf{Q}^\dagger$ is diagonal by examining the off-diagonal elements. Note that each

off-diagonal matrix ($\forall i \neq j$) in (12), $\mathbf{H}_i\mathbf{H}_j^{\dagger}$, can be expanded as

$$\mathbf{H}_i\mathbf{H}_j^{\dagger} = \begin{bmatrix} \mathbf{H}_i^{(1)}\mathbf{H}_j^{(1)\dagger} & \mathbf{H}_i^{(1)}\mathbf{H}_j^{(2)\dagger} & \cdots & \mathbf{H}_i^{(1)}\mathbf{H}_j^{(\frac{2L-1}{D})\dagger} \\ \mathbf{H}_i^{(2)}\mathbf{H}_j^{(1)\dagger} & \mathbf{H}_i^{(2)}\mathbf{H}_j^{(2)\dagger} & \cdots & \mathbf{H}_i^{(2)}\mathbf{H}_j^{(\frac{2L-1}{D})\dagger} \\ \vdots & \vdots & \ddots & \cdots \\ \mathbf{H}_i^{(\frac{2L-1}{D})}\mathbf{H}_j^{(1)\dagger} & \mathbf{H}_i^{(\frac{2L-1}{D})}\mathbf{H}_j^{(2)\dagger} & \cdots & \mathbf{H}_i^{(\frac{2L-1}{D})}\mathbf{H}_j^{(\frac{2L-1}{D})\dagger} \end{bmatrix}. \tag{14}$$

From (14), we can see that each element of $\mathbf{H}_i\mathbf{H}_j^{\dagger}$, $\left[\mathbf{H}_i\mathbf{H}_j^{\dagger}\right]_{m,n} = \mathbf{H}_i^{(m)}\mathbf{H}_j^{(n)\dagger}$, is the sum of multiple independent random variables. Therefore, when K_{max} is sufficiently large, $\left[\mathbf{H}_i\mathbf{H}_j^{\dagger}\right]_{m,n}$ can be regarded as a Gaussian random variable, whose distribution is completely determined by first and second moment.

Based on the independence between the channel taps and distinct receivers, it is obvious that

$$\mathbb{E}\left[\mathbf{H}_i^{(m)}\mathbf{H}_j^{(n)\dagger}\right] = 0, \tag{15}$$

while the second moment can be upper bounded as follows

$$\begin{aligned} \mathbb{E}\left[|\mathbf{H}_i^{(m)}\mathbf{H}_j^{(n)\dagger}|^2\right] &\overset{(a)}{=} \sum_{l=1}^{L} \mathbb{E}\left[|\mathbf{H}_i^{(m)}(l)|^2|\mathbf{H}_j^{(n)}(l)|^2\right], \\ &\overset{(b)}{\leq} \sum_{l=1}^{L} \mathbb{E}\left[|\mathbf{H}_i^{(\frac{L}{D})}(l)|^2\right]\mathbb{E}\left[|\mathbf{H}_j^{(\frac{L}{D})}(l)|^2\right], \\ &\overset{(c)}{=} \frac{\left(\sum_{k=1}^{K_{max}}\sigma_k^2\right)^2}{L}, \end{aligned} \tag{16}$$

where (a) is obtained directly from the independence, (b) is based on the matrix structure in (8) and (c) comes from the fact that the K_{max} multipaths are randomly distributed among the L-tap channel and thus

$$\mathbb{E}\left[|h_j(m)|^2\right] = \mathbb{E}\left[|h_j(n)|^2\right] = \frac{\sum_{k=1}^{K_{max}}\sigma_k^2}{L} \quad \forall m, n. \tag{17}$$

Note $\sum_{k=1}^{K_{max}}\sigma_k^2 < K_{max}$ due to the pass loss attenuation. Therefore, (c) will converge to 0 given $L/K_{max}^p \to c$ where $p > 2$. From (15) and (16), we can conclude that

$$\lim_{K_{max}\to\infty}\left[\mathbf{H}_i\mathbf{H}_j^{\dagger}\right]_{m,n} = 0, \forall m, n, and\ i \neq j. \tag{18}$$

Next, let us examine the diagonal submatrix of $\mathbf{Q}\mathbf{Q}^{\dagger}$, which can be expanded as

$$\mathbf{H}_j\mathbf{H}_j^{\dagger} = \begin{bmatrix} \mathbf{H}_j^{(1)}\mathbf{H}_j^{(1)\dagger} & \mathbf{H}_j^{(1)}\mathbf{H}_j^{(2)\dagger} & \cdots & \mathbf{H}_j^{(1)}\mathbf{H}_j^{(\frac{2L-1}{D})\dagger} \\ \mathbf{H}_j^{(2)}\mathbf{H}_j^{(1)\dagger} & \mathbf{H}_j^{(2)}\mathbf{H}_j^{(2)\dagger} & \cdots & \mathbf{H}_j^{(2)}\mathbf{H}_j^{(\frac{2L-1}{D})\dagger} \\ \vdots & \vdots & \ddots & \cdots \\ \mathbf{H}_j^{(\frac{2L-1}{D})}\mathbf{H}_j^{(1)\dagger} & \mathbf{H}_j^{(\frac{2L-1}{D})}\mathbf{H}_j^{(2)\dagger} & \cdots & \mathbf{H}_j^{(\frac{2L-1}{D})}\mathbf{H}_j^{(\frac{2L-1}{D})\dagger} \end{bmatrix}. \tag{19}$$

Similarly, each element $\left[\mathbf{H}_j\mathbf{H}_j^{\dagger}\right]_{m,n} = \mathbf{H}_j^{(m)}\mathbf{H}_j^{(n)\dagger}$ can be regarded as Gaussian variable when K_{max} is sufficiently large. Since $\mathbf{H}_j^{(m)}$ and $\mathbf{H}_j^{(n)}$ are independent when $m \neq n$, similar to (15) and (16), we can derive

$$\begin{cases} \mathbb{E}\left[\mathbf{H}_j^{(m)}\mathbf{H}_j^{(n)\dagger}\right] & = 0 \quad m \neq n, \\ \mathbb{E}\left[|\mathbf{H}_j^{(m)}\mathbf{H}_j^{(n)\dagger}|^2\right] & \leq \frac{\left(\sum_{k=1}^{K_{max}}\sigma_k^2\right)^2}{L} \quad m \neq n, \end{cases} \tag{20}$$

and given $L/K_{max}^p \to c$ where $p > 2$, we have derived that

$$\lim_{K_{max}\to\infty}\left[\mathbf{H}_j\mathbf{H}_j^{\dagger}\right]_{m,n} = 0, \forall j, and\ m \neq n. \tag{21}$$

Therefore, we can conclude that $\mathbf{Q}\mathbf{Q}^{\dagger}$ is diagonal. This completes the proof. ■

The assumption that $K_{max} \to \infty$ is just for analyzing the asymptotical achievable rate of the TR system as the assumption $M_t \to \infty$ in early massive MIMO works. In practice, we only need that K_{max} is large enough to achieve massive multipath effect. Based on the real indoor measurement in Sec. VI.B, we have demonstrated that the number of the resolved multipaths in a typical indoor environment is large enough given a sufficiently large bandwidth. Even though K_{max} is a fixed value given the power and environment, there still exists other method to realize massive multipaths. Since the TR and MIMO technology are not mutually exclusive, the independent multipaths can be easily scaled up by adding a few antennas. How to realize massive multipaths is discussed with real indoor measurement later in Section VI.

V. Expected Achievable Rate under Different Signature Waveforms

In this section, we analyze the expected achievable rate under three different designs of signature waveform: basic TR signature [25], ZF signature [41] and MMSE signature [30]. With utilization of TRMME in Section IV, the asymptotical achievable rate with three signature waveforms is further derived.

A. Expected Achievable Rate

The three signature waveforms are shown in the following,

$$\mathbf{g}_j = \begin{cases} \mathbf{H}_j^{(L/D)\dagger}/\|\mathbf{H}_j^{(L/D)}\|, & \text{Basic TR} \\ c_{ZF}\mathbf{Q}^\dagger(\mathbf{Q}\mathbf{Q}^\dagger)^{-1}\mathbf{e}_{l_j}, & \text{ZF} \\ c_{MMSE}(\mathbf{Q}^\dagger\mathbf{Q}+\frac{1}{p_u}\mathbf{I})^{-1}\mathbf{Q}^\dagger\mathbf{e}_{l_j}, & \text{MMSE} \end{cases} \tag{22}$$

where c_{ZF} and c_{MMSE} are normalization constants, $\mathbf{Q} = [\mathbf{H}_1^T, \mathbf{H}_2^T, \cdots, \mathbf{H}_N^T]^T$, $\mathbf{e}_{l_j}$ is an elementary vector with $l_j = (j-1)(2L-1)/D + L/D$, $\mathbf{I}$ is the identity matrix, and p_u is the transmitting signal-to-noise ratio (SNR) of each user defined as

$$p_u = \frac{P}{NP_n}. \tag{23}$$

With the definition of $\mathbf{Q}$ and $\mathbf{e}_{l_j}$ above, we have

$$\mathbf{Q}^\dagger\mathbf{e}_{l_j} = \mathbf{H}_j^{(L/D)\dagger}. \tag{24}$$

Note that under the multipath-rich scenario, ZF signature can completely cancel out the interference given large amount of independent multipaths. In addition, MMSE signature has a simpler closed form solution with the fixed dual uplink power allocation [30].

Theorem 1 (Expected Achievable Rate): The expected achievable rate of the TR system with basic TR signature, ZF signature, and MMSE signature can be written as follows

$$\begin{aligned} R_j^{Basic} &= \frac{W}{D}\mathbb{E}\left[\log_2\left(1+\frac{p_u\|\mathbf{h}_j\|^4}{p_u([\mathbf{Q}\mathbf{Q}^\dagger\mathbf{Q}\mathbf{Q}^\dagger]_{l_j,l_j}-\|\mathbf{h}_j\|^4)+\|\mathbf{h}_j\|^2}\right)\right], \\ R_j^{ZF} &= \frac{W}{D}\mathbb{E}\left[\log_2\left(1+\frac{p_u}{[(\mathbf{Q}\mathbf{Q}^\dagger)^{-1}]_{l_j,l_j}}\right)\right], \\ R_j^{MMSE} &= \frac{W}{D}\mathbb{E}\left[\log_2\left(\frac{1}{\left[(\mathbf{I}+p_u\mathbf{Q}\mathbf{Q}^\dagger)^{-1}\right]_{l_j,l_j}}\right)\right]. \end{aligned} \tag{25}$$

The proof for Theorem 1 is listed in the appendix. Even though (25) seems similar to those for MIMO MRC/ZF/MMSE receivers, the matrix $\mathbf{Q}$ is different from the channel profile matrix in MIMO system, which results in significantly different derivation of the asymptotical performance in the TR system. More specifically, due to the large channel delay spread in the TR system, there exists ISI. Therefore, backoff factor D is adopted in our paper and the channel profile $\mathbf{H}_i$ becomes the decimated Toeplitz matrix, which is much more complicated than that in MIMO system.

Actually combined with channel model in Section II, the derivation of the expected asymptotical performance relies on more advanced techniques from random matrix theory. Furthermore, it is the first work analyzing the asymptotical achievable rate for TR system with various signature design methods with considering the ISI in practical system.

From Theorem 1, we can see that the expressions of expected achievable rate under different signatures are closely related to $\mathbf{Q}\mathbf{Q}^\dagger$ and $\left[\mathbf{Q}\mathbf{Q}^\dagger\mathbf{Q}\mathbf{Q}^\dagger\right]_{l_j,l_j}$. Actually, the asymptotical property of $\mathbf{Q}\mathbf{Q}^\dagger$ has been studied previously as the TRMME. In the following section, we will further explore the property of $\left[\mathbf{Q}\mathbf{Q}^\dagger\mathbf{Q}\mathbf{Q}^\dagger\right]_{l_j,l_j}$ under a massive multipath setting, i.e., when $K_{max}\to\infty$, and study the corresponding asymptotic expected achievable rate with different signatures.

B. Asymptotic Performance

From Theorem 1, we can see that the expected achievable rate with the basic TR signature depends on $\left[\mathbf{Q}\mathbf{Q}^\dagger\mathbf{Q}\mathbf{Q}^\dagger\right]_{l_j,l_j}$. Therefore, we derive the asymptotic property of $\left[\mathbf{Q}\mathbf{Q}^\dagger\mathbf{Q}\mathbf{Q}^\dagger\right]_{l_j,l_j}$ in the following Lemma. After that, we derive the asymptotical achievable rate in the TR system given massive multipaths.

Lemma 1: Under the asymptotic setting where $K=K_{max}\to\infty$, we have

$$\frac{\left[\mathbf{Q}\mathbf{Q}^\dagger\mathbf{Q}\mathbf{Q}^\dagger\right]_{l_j,l_j}-\|\mathbf{h}_j\|^4}{\sum_{k=1}^{K_{max}}\sigma_k^2}\overset{d}{\leq}\alpha \tag{26}$$

where $\alpha=2N/D$.

Proof: With the definition of $\mathbf{Q}$ and (9), we have

$$\begin{aligned}&\left[\mathbf{Q}\mathbf{Q}^\dagger\mathbf{Q}\mathbf{Q}^\dagger\right]_{l_j,l_j}-\|\mathbf{h}_j\|^4=\\&\sum_{i=1,i\neq j}^{N}\sum_{l=1}^{(2L-1)/D}|\mathbf{H}_i^{(l)}\mathbf{H}_j^{(\frac{L}{D})\dagger}|^2+\sum_{l=1,l\neq(L/D)}^{(2L-1)/D}|\mathbf{H}_j^{(l)}\mathbf{H}_j^{(\frac{L}{D})\dagger}|^2,\end{aligned} \tag{27}$$

which is the sum of multiple independent random variables. Therefore, $\left[\mathbf{Q}\mathbf{Q}^\dagger\mathbf{Q}\mathbf{Q}^\dagger\right]_{l_j,l_j}-\|\mathbf{h}_j\|^4$ can be regarded as a Guassian random variable when K_{max} is sufficiently large.

Similar to (16), we have the following

$$\begin{cases}\mathbb{E}\left[|\mathbf{H}_i^{(l)}\mathbf{H}_j^{(\frac{L}{D})\dagger}|^2\right] & \leq\frac{\left(\sum_{k=1}^{K_{max}}\sigma_k^2\right)^2}{L} \quad i\neq j,\\ \mathbb{E}\left[|\mathbf{H}_j^{(l)}\mathbf{H}_j^{(\frac{L}{D})\dagger}|^2\right] & \leq\frac{\left(\sum_{k=1}^{K_{max}}\sigma_k^2\right)^2}{L} \quad l\neq(L/D).\end{cases} \tag{28}$$

Therefore, with $K_{max} \to \infty$, the expectation of $\left[\mathbf{Q}\mathbf{Q}^{\dagger}\mathbf{Q}\mathbf{Q}^{\dagger}\right]_{l_j,l_j} - \|\mathbf{h}_j\|^4$ can be bounded by

$$\begin{aligned} &\mathbb{E}\left[\left[\mathbf{Q}\mathbf{Q}^{\dagger}\mathbf{Q}\mathbf{Q}^{\dagger}\right]_{l_j,l_j} - \|\mathbf{h}_j\|^4\right] \\ &\leq \frac{N(2L-1)}{D}\frac{\left(\sum_{k=1}^{K_{max}}\sigma_k^2\right)^2}{L}, \\ &\leq \alpha\left(\sum_{k=1}^{K_{max}}\sigma_k^2\right)^2, \end{aligned} \tag{29}$$

with $\alpha = 2N/D$.

Similar to the argument in the derivation of (17), the fourth moment of $h_j(m)$ can be given as

$$\mathbb{E}\left[|h_j(m)|^4\right] = \mathbb{E}\left[|h_j(n)|^4\right] = 2\left(\frac{\sum_{k=1}^{K_{max}}\sigma_k^2}{L}\right)^2 \quad \forall m, n. \tag{30}$$

Then, we have,

$$\begin{cases} \mathbb{E}\left[|\mathbf{H}_i^{(l)}\mathbf{H}_j^{(\frac{L}{D})\dagger}|^4\right] & \leq \frac{4\left(\sum_{k=1}^{K_{max}}\sigma_k^2\right)^4}{L^3} \quad i \neq j \\ \mathbb{E}\left[|\mathbf{H}_j^{(l)}\mathbf{H}_j^{(\frac{L}{D})\dagger}|^4\right] & \leq \frac{4\left(\sum_{k=1}^{K_{max}}\sigma_k^2\right)^4}{L^3} \quad l \neq (L/D) \end{cases} \tag{31}$$

As $K_{max} \to \infty$, $L/K_{max}^p \to c$ where $p > 2$ holds in the multipath-rich scenario. Therefore, the variance of $\left[\mathbf{Q}\mathbf{Q}^{\dagger}\mathbf{Q}\mathbf{Q}^{\dagger}\right]_{l_j,l_j} - \|\mathbf{h}_j\|^4$ goes to zero as $K_{max} \to \infty$. Combining the first moment in (29), we can derive the result in Lemma 1. This completes the proof. ■

Remark: In a massive MIMO system, when the number of antennas grows large, the random channel vectors between the users and the base station become pairwisely orthogonal [45]. Similarly, in a TR system, when the number of multipaths grows large, a pairwisely orthogonal property among the random channel vectors between the receivers and the transmitter exists, as shown in the TRMME. On the other hand, while, in a massive MIMO system, simple matched filter processing can completely remove the uncorrelated noise and interference with an infinite number of antennas [4], due to the existence of ISI in a TR system, the basic TR signature cannot completely remove the interference in general. Therefore, Lemma 1 is needed for the derivation of the asymptotic expected achievable rate for the TR system with basic TR signature.

Based on the TRMME and Lemma 1, we can analyze the asymptotic expected achievable rate under different signatures, and the results are summarized in the following Theorem.

Theorem 2: When $K_{max} \to \infty$, the asymptotic expected achievable rate with the ZF signature and MMSE signature satisfy that

$$\frac{R_j^{ZF}}{W/D} = \frac{R_j^{MMSE}}{W/D} = \mathbb{E}\left[\log_2\left(1+p_u\|\mathbf{h}_j\|^2\right)\right], \tag{32}$$

while the asymptotic expected achievable rate with the basic TR signature satisfies the following inequality,

$$\frac{R_j^{Basic}}{W/D} \geq \mathbb{E}\left[\log_2\left(1+\frac{p_u\|\mathbf{h}_j\|^2}{\frac{p_u\alpha\left(\sum_{k=1}^{K_{max}}\sigma_k^2\right)^2}{\|\mathbf{h}_j\|^2}+1}\right)\right]. \tag{33}$$

Proof: According to the TRMME, we have

$$\lim_{K_{max}\to\infty}\frac{\left[\left(\mathbf{Q}\mathbf{Q}^\dagger\right)^{-1}\right]_{l_j,l_j}}{\|\mathbf{h}_j\|^2} = 1. \tag{34}$$

Then, according to (50), the asymptotic expected achievable rate under ZF signature is

$$\frac{R_j^{ZF}}{W/D} \to \mathbb{E}\left[\log_2\left(1+p_u\|\mathbf{h}_j\|^2\right)\right]. \tag{35}$$

Similarly, with the TRMME, we can also have

$$\begin{aligned}\left[\left(\mathbf{I}+p_u\mathbf{Q}\mathbf{Q}^\dagger\right)^{-1}\right]_{l_j,l_j} &\to \left[\left(\mathbf{I}+p_u\lambda\right)^{-1}\right]_{l_j,l_j}\\ &= \frac{1}{1+p_u\|\mathbf{h}_j\|^2}\end{aligned} \tag{36}$$

By substituting (36) into (56), the asymptotic expected achievable rate under MMSE signature is

$$\frac{R_j^{MMSE}}{W/D} \to \mathbb{E}\left[\log_2\left(1+p_u\|\mathbf{h}_j\|^2\right)\right]. \tag{37}$$

Finally, by substituting (26) of Lemma 1 into (46), the asymptotic expected achievable rate under basic TR signature can be lower bounded as

$$\frac{R_j^{Basic}}{W/D} \geq \mathbb{E}\left[\log_2\left(1+\frac{p_u\|\mathbf{h}_j\|^2}{\frac{p_u\alpha\left(\sum_{k=1}^{K_{max}}\sigma_k^2\right)^2}{\|\mathbf{h}_j\|^2}+1}\right)\right]. \tag{38}$$

This completes the proof. ■

From Theorem 2, we can see that the ZF and MMSE signatures generally outperform the basic TR signature in terms of expected achievable rate. However, when D is sufficiently large so that $\frac{\alpha\left(\sum_{k=1}^{K_{max}}\sigma_k^2\right)^2}{\|\mathbf{h}_j\|^2}$ goes to zero, this is the case when the ISI and IUI are eliminated, then the basic TR signature can achieve the same asymptotic expected achievable rate with ZF and MMSE signatures.

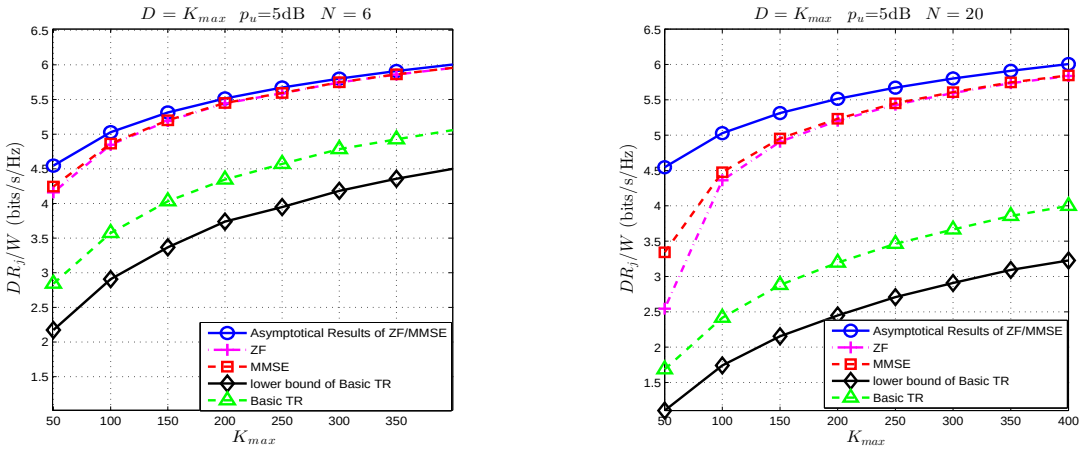

(a) $N = 6$ (b) $N = 20$

Fig. 3: Comparison between the asymptotic performance with varying N, with $D = K_{max}$ and $p_u = 5$dB.

VI. Simulations and Experiments

In this section, we conduct simulations and experiments to evaluate the expected asymptotical performance of a TR system under various settings. We assume that the N receivers are uniformly, randomly distributed and share the same channel model, which is discussed in Section III. Since more received power will be captured within the multipath-rich environment, we assume the expected channel gain as an increasing function of the number of independent multipaths K_{max}.

A. Asymptotical Performance

We first validate our theoretical analysis in Theorem 2. The y-axis is DR_j/W, where R_j is the expected achievable rate of the j^{th} receiver, D is the backoff factor and W is the system bandwidth. Since the channel gain is assumed to be an increasing function of K_{max}, the asymptotical performance would increase with K_{max} as well. The case when D is not sufficiently large, e.g., $D = K_{max}$ is first investigated. The expected asymptotical performance of each receiver is shown in Fig. 3 with $p_u = 5$dB and different N. From Fig. 3, we can observe that the performance using ZF and MMSE signatures converges to the same limit quickly as K_{max} increases. Also, there is a gap between the asymptotic limit of ZF/MMSE signature and

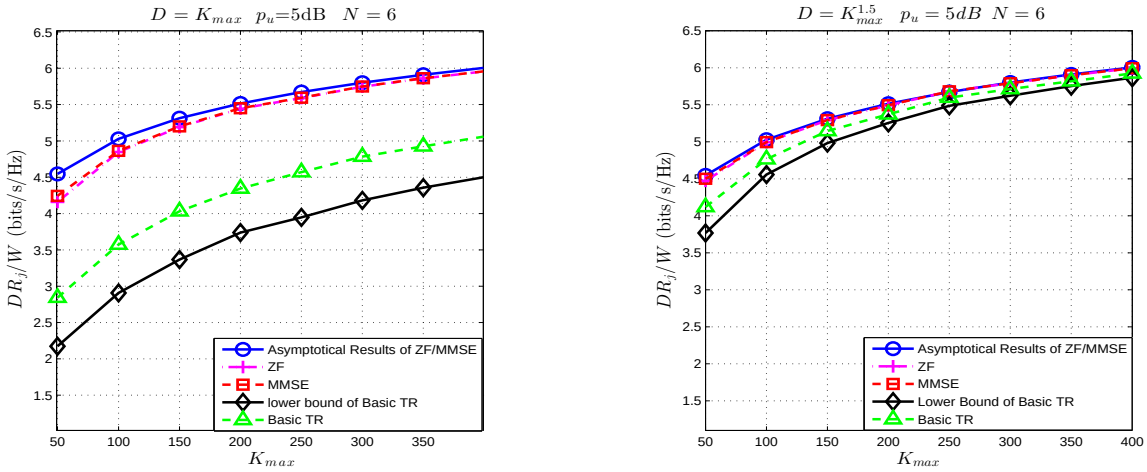

(a) $D = K_{max}$ (b) $D = K_{max}^{1.5}$

Fig. 4: Comparison between the asymptotic performance with varying D, with $N = 6$ and $p_u = 5$dB.

the lower bound of the basic TR signature. This is mainly because when the basic TR signature is used and the D is not large enough, there exists residual ISI and IUI and $\frac{\alpha\left(\sum_{k=1}^{K_{max}} \sigma_k^2\right)^2}{\|\mathbf{h}_j\|^2}$ cannot be negligible. By comparing the results with $N = 6$ and $N = 20$, we notice that the gap becomes even larger when N increases, which is due to the increase of $\alpha = 2N/D$.

We also compare the asymptotical performance of basic TR, ZF and MMSE signatures by varying D. It can be seen in Fig. 4 that the gap between the asymptotic performance of ZF/MMSE signature and that of the basic TR signature becomes much smaller when D and K_{max} are both sufficiently larger. Such a phenomenon is mainly due to less severe ISI and IUI and a much smaller $\frac{\alpha\left(\sum_{k=1}^{K_{max}} \sigma_k^2\right)^2}{\|\mathbf{h}_j\|^2}$. Therefore, the basic TR signature can achieve the same optimal asymptotic expected achievable rate with ZF and MMSE signatures with sufficiently large D.

B. The Number of Observable Independent Multipaths K in a Typical Indoor Environment

To achieve the asymptotic performance in Theorem 2 requires the TR system to operate in a multipath-rich environment. In this subsection, we investigate the property of K in a typical indoor environment using real-world measurements. First, we demonstrate that, in a typical office, the number of resolvable multipaths is large with a sufficiently large bandwidth. Then,

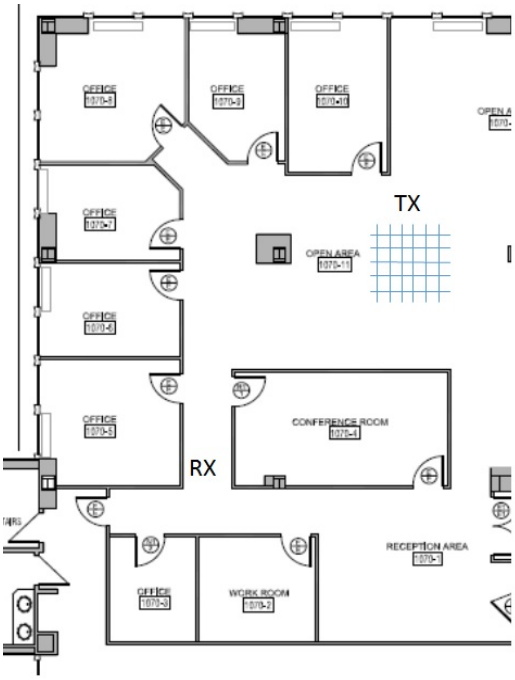

Fig. 5: Floor Plan

the approach to increase K_{max} is further discussed and validated through real measurements.

We use two Universal Software Radio Peripherals (USRPs) as channel sounders to probe the channel in a typical office room, whose floor plan is shown in Fig. 5. As shown in the figure, TX is placed on a grid structure with 5cm resolution and RX is placed at the corner. With two USRPs, we scan the spectrum, e.g., from 4.9GHz to 5.9GHz, to acquire the channel impulse response with a bandwidth of 10MHz-1GHz.

We employ eigenvalue analysis to determine the value of K for any given bandwidth W. First, we estimate the covariance matrix of the measured channels $\mathbf{K}_{h,W}$ using statistical averaging

$$\mathbf{K}_{h,W} = \frac{1}{N}\sum_{i=1}^{N} \mathbf{h}_{i,W}\mathbf{h}_{i,W}^{\dagger}, \tag{39}$$

where $\mathbf{h}_{i,W}$ is the channel information obtained at location i with bandwidth W and $N = 100$. Since $\mathbf{K}_{h,W}$ is Hermitian and positive definite, there exists a unitary matrix U such that

$$\mathbf{K}_{h,W} = U\Lambda U^{\dagger} = \sum_{i=1}^{L} \lambda_{i,W}\psi_i\psi_i^{\dagger}, \tag{40}$$

where $\lambda_{1,W} \geq \lambda_{2,W} \geq \cdots \geq \lambda_{L,W}$ and $L = \tau_C W$.

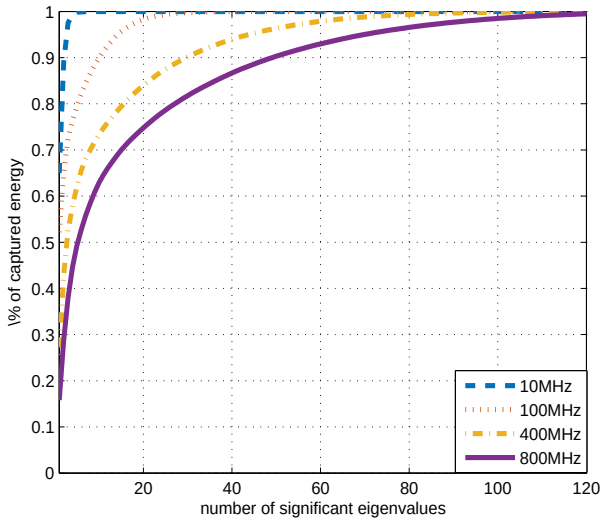

Fig. 6: Percentage of captured energy versus the number of significant eigenvalues with a single antenna

In Fig. 6, we show the percentage of the captured energy E_l versus the number of significant eigenvalues l, with E_l defined as $E_l = \frac{\sum_{i=1}^{l} \lambda_i}{\sum_{i=1}^{L} \lambda_i}$. From Fig. 6, we can see that the channel energy is concentrated in a small number of eigenvalues when the bandwidth is small, while spread over a large number of eigenvalues as the bandwidth increases. In other words, the degree of freedom K increases as the bandwidth W increases. This is further confirmed in Fig. 7, where we show the number of significant eigenvalues versus the channel bandwidth by fixing the captured energy at 98%.

From previous measurements, K_{max} is a large value in a typical indoor environment. Now we discuss an approach to further increase K_{max} in practical environment. Since the TR and MIMO technology are not mutually exclusive, the degree of freedom can be further scaled up by deploying a couple antennas to harvest hundreds of virtual antennas as shown in Fig. 7. As indicated in the figure, it would be easy to realize massive virtual antennas with a few antennas in the TR system instead of installing hundreds of physical antennas.

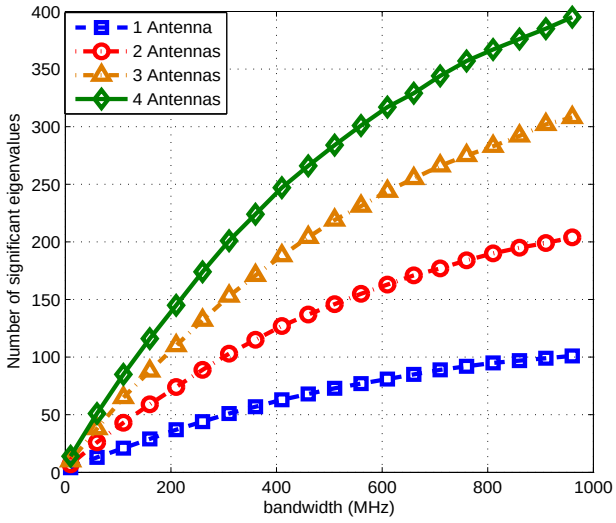

Fig. 7: Number of significant eigenvalues K at different bandwidth W

C. Comparison with Massive MIMO

The assumption that $K_{max} \to \infty$ is just for analyzing the asymptotical achievable rate of the TR system as the assumption $M_t \to \infty$ in early massive MIMO works. In practice, we only need that K_{max} is large enough to achieve massive multipath effect. In the following, we will demonstrate that even with a single antenna, TR wideband system is still capable to reach comparable achievable rate with massive MIMO system based on our indoor experiment. Our experiment is conducted with the real indoor channel measurement and the achievable rate in TR system is calculated based on Theorem 1.

In this subsection, we first evaluate the expected achievable rate of the TR system in a typical indoor environment using the channel measurements in the previous subsection, with $W = 1$GHz. Then we compare the performance of the TR system with that of a massive MIMO system. Clearly, there is a tradeoff in selecting a proper D: W/D will decrease as D increases, while both the ISI and IUI get reduced as D increases. In Fig. 8 we show the the expected achievable rate of different signature waveforms with different D.

We can see that the expected achievable rate of the basic TR signature saturates quickly as p_u increases because it is interference-limited with $N = 10$ receivers. Increasing D may decrease the expected achievable rate for the basic TR signature if the decrease in W/D dominates the

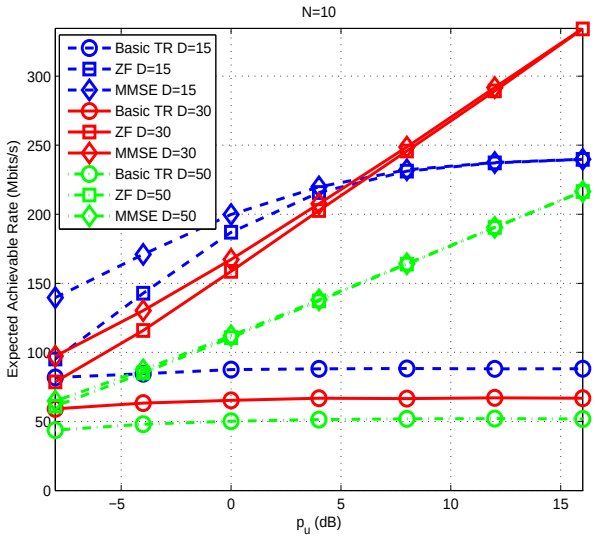

Fig. 8: Expected achievable rate by varying the backoff factor D, with $N = 10$ and $W = 1$GHz.

increase in SINR for a relatively large D as shown in Fig. 8. The expected achievable rates of ZF and MMSE signatures also saturate at high p_u with $D = 15$, but can be improved by increasing D, e.g. $D = 30$, to reduce the interference. However, it may hurt the rate performance if we increase D too much, e.g., $D = 50$.

We choose $D = 30$ as the backoff factor used in a TR system and compare the expected achievable rates using ZF and MMSE signatures to that of a genie-aided massive MIMO system, where "genie-aided" means the interference, antenna coupling effects and the loss due to cyclic prefix are ignored. Assume the genie-aided massive MIMO system has a bandwidth W_{MM} and M antennas at the transmitter, then user j's expected achievable rate can be calculated as [3]

$$\mathbf{R}_j^{MM} = W_{MM}\mathbb{E}\left[\log_2\left(1 + p_u\|\widehat{\mathbf{h}}_j\|^2\right)\right] \quad (bits/s), \tag{41}$$

where W_{MM} is chosen as 20MHz according to the massive MIMO prototype [9].

Note that massive MIMO has high spectral efficiency by utilizing a large amount of antennas, which however leads to the complexity and cost of hardware implementation. On the other hand, the spectral efficiency of TR system is much lower since the large bandwidth is utilized to harvest the multipaths and lower down the cost and complexity. Considering the potential wide bandwidth available in future (e.g., UWB and mmWave band), the complexity, energy consumption and other metrics become more and more important compared with the spectral

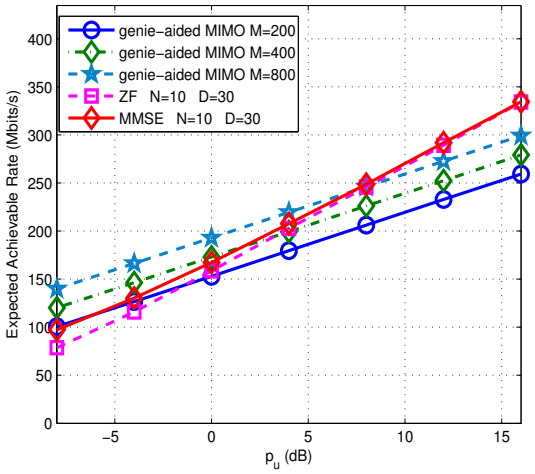

(a) Expected achievable rate comparison between TR and massive MIMO systems, with $W = 1GHz$, $N = 10$ and $D = 30$ for the TR system, and $W_{MM} = 20MHz$.

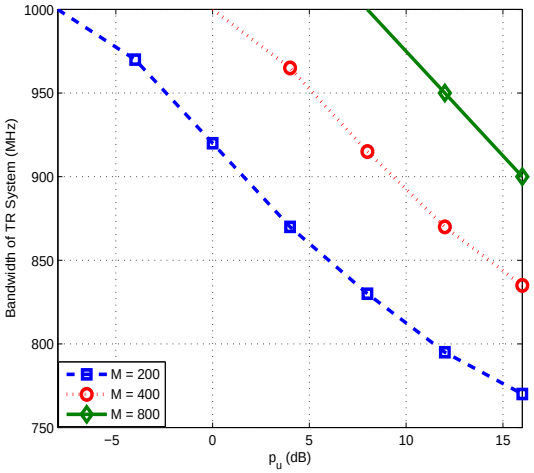

(b) Bandwidth requirement of TR system with MMSE signature to achieve the same achievable rate of a massive MIMO system with $W_{MM} = 20MHz$.

Fig. 9: Comparison of the achievable rate in TR and massive MIMO system

efficiency given the comparable achievable can be achieved as shown in Fig. 9a. Moreover, the bandwidth requirement for TR system to achieve the same achievable rate with a massive MIMO system (with hundreds of antennas and 20MHz bandwidth) is shown in Fig. 9b. As shown in Fig. 9b, to achieve the same achievable rate as a massive MIMO system with a larger number of antennas, a larger bandwidth is required by the TR system. Note that the performance of TR is obtained from real data, while that of massive MIMO is the best case scenario. Another note is the one requires a large number of antennas, while the other larger bandwidth.

VII. Conclusion

In this paper, we demonstrate that the TR technology, through harvesting the naturally existing virtual antennas, can offer a cost effective solution to achieve the desired massive MIMO performance demanded in the possible future 5G systems. We derive the achievable rate of the TR system with basic TR, ZF, and MMSE signatures under the asymptotic limiting settings. We prove theoretically and validate with simulations that the TR system with ZF and MMSE signatures can asymptotically achieve the limiting achievable rate, where the interference is completely

eliminated. When the backoff factor is sufficiently large, the basic TR signature can also achieve the same asymptotic achievable rate. Finally, based on the real channel measurements, experiment is conducted to show that the single-antenna TR wideband system can achieve comparable rates as that of the massive MIMO system. Note that by utilizing the environment as virtual antenna array and computing resource, the implementation complexity of the TR system is much lower. What a TR system needs is large enough bandwidth to harvest multipaths in the environment. With highspeed ADC becoming more affordable, wider bandwidth is readily available. On the contrary, the huge number of antennas demanded by a massive MIMO system may continue to face the challenge of unavoidable coupling effects.

APPENDIX

A. Expected Achievable Rate under Basic TR Signature

From (22), the basic TR signature is $\mathbf{g}_j = \mathbf{H}_j^{(L/D)\dagger}/\|\mathbf{H}_j^{(L/D)}\|$. Therefore, we have

$$\mathbf{g}_j^\dagger \mathbf{H}_j^{(\frac{L}{D})\dagger} \mathbf{H}_j^{(\frac{L}{D})} \mathbf{g}_j = \|\mathbf{H}_j^{(\frac{L}{D})}\|^2, \tag{42}$$

and

$$\mathbf{g}_j^\dagger \left(\sum_{i=1}^{N} \mathbf{H}_i^\dagger \mathbf{H}_i \right) \mathbf{g}_j = \frac{\mathbf{H}_j^{(\frac{L}{D})} \mathbf{Q}^\dagger \mathbf{Q} \mathbf{H}_j^{(\frac{L}{D})\dagger}}{\|\mathbf{H}_j^{(\frac{L}{D})}\|^2}. \tag{43}$$

According to the definition of $\mathbf{H}_j^{(L/D)}$, we have $\|\mathbf{H}_j^{(\frac{L}{D})}\|^2 = \|\mathbf{h}_j\|^2$, and $\mathbf{H}_j^{(L/D)}$ is the $(L/D)^{th}$ row of $\mathbf{H}_j$ and thus l_j^{th} row of $\mathbf{Q}$. Therefore, (42) and (43) can be re-written as

$$\mathbf{g}_j^\dagger \mathbf{H}_j^{(\frac{L}{D})\dagger} \mathbf{H}_j^{(\frac{L}{D})} \mathbf{g}_j = \|\mathbf{h}_j\|^2, \tag{44}$$

and

$$\mathbf{g}_j^\dagger \left(\sum_{i=1}^{N} \mathbf{H}_i^\dagger \mathbf{H}_i \right) \mathbf{g}_j = \frac{\left[\mathbf{Q}\mathbf{Q}^\dagger \mathbf{Q}\mathbf{Q}^\dagger\right]_{l_j,l_j}}{\|\mathbf{h}_j\|^2}, \tag{45}$$

where $[\,\cdot\,]_{l_j,l_j}$ is the (l_j, l_j) element of the matrix.

Substituting (44) and (45) into (10), the expected achievable rate of j^{th} receiver with the basic TR signature can be written as

$$R_j^{Basic} = \frac{W}{D} \mathbb{E}\left[\log_2 \left(1 + \frac{p_u \|\mathbf{h}_j\|^4}{p_u([\mathbf{Q}\mathbf{Q}^\dagger \mathbf{Q}\mathbf{Q}^\dagger]_{l_j,l_j} - \|\mathbf{h}_j\|^4) + \|\mathbf{h}_j\|^2} \right) \right]. \tag{46}$$

B. Expected Achievable Rate under ZF Signature

With the ZF signature $\mathbf{g}_j = c_{ZF}\mathbf{Q}^\dagger(\mathbf{Q}\mathbf{Q}^\dagger)^{-1}\mathbf{e}_{l_j}$, we have

$$\begin{bmatrix} \mathbf{H}_1\mathbf{g}_j \\ \vdots \\ \mathbf{H}_N\mathbf{g}_j \end{bmatrix} = \mathbf{Q}\mathbf{g}_j = c_{ZF}\mathbf{Q}\mathbf{Q}^\dagger(\mathbf{Q}\mathbf{Q}^\dagger)^{-1}\mathbf{e}_{l_j} = c_{ZF}\mathbf{e}_{l_j}. \tag{47}$$

According to (47), we can derive the following

$$\mathbf{g}_j^\dagger\mathbf{H}_i^\dagger\mathbf{H}_i\mathbf{g}_j = \begin{cases} 0, & \forall i \neq j; \\ \mathbf{g}_j^\dagger\mathbf{H}_j^{(\frac{L}{D})\dagger}\mathbf{H}_j^{(\frac{L}{D})}\mathbf{g}_j = c_{ZF}^2, & i = j. \end{cases} \tag{48}$$

Substituting (48) into (10), we can see that both the ISI and IUI are eliminated, and thus the expected achievable rate with ZF signature can be written as

$$R_j^{ZF} = \frac{W}{D}\mathbb{E}\left[\log_2\left(1 + p_u c_{ZF}^2\right)\right]. \tag{49}$$

Since $\mathbf{g}_j^\dagger\mathbf{g}_j = c_{ZF}^2[(\mathbf{Q}\mathbf{Q}^\dagger)^{-1}]_{l_j,l_j} = 1$, the expected achievable rate with ZF signature in (49) can be re-written as

$$R_j^{ZF} = \frac{W}{D}\mathbb{E}\left[\log_2\left(1 + \frac{p_u}{[(\mathbf{Q}\mathbf{Q}^\dagger)^{-1}]_{l_j,l_j}}\right)\right]. \tag{50}$$

C. Expected Achievable Rate under MMSE Signature

According to (22) and the Woodbury matrix identity [46], the MMSE signature can be written as

$$\begin{aligned} \mathbf{g}_j &= c_{MMSE}\left(\mathbf{Q}^\dagger\mathbf{Q} + \frac{1}{p_u}\mathbf{I}\right)^{-1}\mathbf{H}_j^{(\frac{L}{D})\dagger}, \\ &= \frac{c_{MMSE}\Lambda_j^{-1}\mathbf{H}_j^{(\frac{L}{D})\dagger}}{\mathbf{H}_j^{(\frac{L}{D})}\Lambda_j^{-1}\mathbf{H}_j^{(\frac{L}{D})\dagger} + 1}, \end{aligned} \tag{51}$$

where $\Lambda_j \triangleq \mathbf{Q}^\dagger\mathbf{Q} - \mathbf{H}_j^{(\frac{L}{D})\dagger}\mathbf{H}_j^{(\frac{L}{D})} + (1/p_u)\mathbf{I}$.

By multiplying both sides in (51) with $\mathbf{H}_j^{(\frac{L}{D})}$, we can derive the following

$$\mathbf{H}_j^{(\frac{L}{D})}\Lambda_j^{-1}\mathbf{H}_j^{(\frac{L}{D})\dagger} = \frac{1}{1 - \mathbf{H}_j^{(\frac{L}{D})}\left(\mathbf{Q}^\dagger\mathbf{Q} + \frac{1}{p_u}\mathbf{I}\right)^{-1}\mathbf{H}_j^{(\frac{L}{D})\dagger}} - 1. \tag{52}$$

Moreover, according to (51), we have

$$\mathbf{g}_j^\dagger \mathbf{H}_j^{(\frac{L}{D})\dagger} \mathbf{H}_j^{(\frac{L}{D})} \mathbf{g}_j = \frac{c_{MMSE}^2 \left(\mathbf{H}_j^{(\frac{L}{D})} \Lambda_j^{-1} \mathbf{H}_j^{(\frac{L}{D})\dagger} \right)^2}{\left(\mathbf{H}_j^{(\frac{L}{D})} \Lambda_j^{-1} \mathbf{H}_j^{(\frac{L}{D})\dagger} + 1 \right)^2}, \tag{53}$$

and

$$\mathbf{g}_j^\dagger \Lambda_j \mathbf{g}_j = \frac{c_{MMSE}^2 \mathbf{H}_j^{(\frac{L}{D})} \Lambda_j^{-1} \mathbf{H}_j^{(\frac{L}{D})\dagger}}{\left(\mathbf{H}_j^{(\frac{L}{D})} \Lambda_j^{-1} \mathbf{H}_j^{(\frac{L}{D})\dagger} + 1 \right)^2}. \tag{54}$$

Then, the expected achievable rate in (10) can be re-rewritten as

$$\begin{aligned} R_j^{MMSE} &\overset{(a)}{=} \frac{W}{D} \mathbb{E} \left[\log_2 \left(1 + \frac{\mathbf{g}_j^\dagger \mathbf{H}_j^{(\frac{L}{D})\dagger} \mathbf{H}_j^{(\frac{L}{D})} \mathbf{g}_j}{\mathbf{g}_j^\dagger \left(\mathbf{H}_j^\dagger \mathbf{H}_j - \mathbf{H}_j^{(\frac{L}{D})\dagger} \mathbf{H}_j^{(\frac{L}{D})} + \sum_{i \neq j} \mathbf{H}_i^\dagger \mathbf{H}_i + \frac{1}{p_u} \mathbf{I} \right) \mathbf{g}_j} \right) \right], \\ &\overset{(b)}{=} \frac{W}{D} \mathbb{E} \left[\log_2 \left(1 + \frac{\mathbf{g}_j^\dagger \mathbf{H}_j^{(\frac{L}{D})\dagger} \mathbf{H}_j^{(\frac{L}{D})} \mathbf{g}_j}{\mathbf{g}_j^\dagger \Lambda_j \mathbf{g}_j} \right) \right], \\ &\overset{(c)}{=} \frac{W}{D} \mathbb{E} \left[\log_2 \left(1 + \mathbf{H}_j^{(\frac{L}{D})} \Lambda_j^{-1} \mathbf{H}_j^{(\frac{L}{D})\dagger} \right) \right], \end{aligned} \tag{55}$$

where (a) is the direct result from $\mathbf{g}_j^\dagger \mathbf{g}_j = 1$, (b) comes from the definition of Λ_j, and (c) are based on (53) and (54).

By substituting (52) into (55), the expected achievable rate with MMSE signature can be further simplified as

$$\begin{aligned} R_j^{MMSE} &= \frac{W}{D} \mathbb{E} \left[\log_2 \left(\frac{1}{1 - \mathbf{H}_j^{(\frac{L}{D})} \left(\mathbf{Q}^\dagger \mathbf{Q} + \frac{1}{p_u} \mathbf{I} \right)^{-1} \mathbf{H}_j^{(\frac{L}{D})\dagger}} \right) \right], \\ &= \frac{W}{D} \mathbb{E} \left[\log_2 \left(\frac{1}{1 - \left[\mathbf{Q} \left(\mathbf{Q}^\dagger \mathbf{Q} + \frac{1}{p_u} \mathbf{I} \right)^{-1} \mathbf{Q}^\dagger \right]_{l_j, l_j}} \right) \right], \\ &= \frac{W}{D} \mathbb{E} \left[\log_2 \left(\frac{1}{\left[\left(\mathbf{I} + p_u \mathbf{Q} \mathbf{Q}^\dagger \right)^{-1} \right]_{l_j, l_j}} \right) \right], \end{aligned} \tag{56}$$

where the second equality comes from the definition of $\mathbf{H}_j^{(\frac{L}{D})}$ and the last equality comes from the following derivation by utilizing the Woodbury matrix identity [46],

$$\left(\mathbf{I} + p_u \mathbf{Q} \mathbf{Q}^\dagger \right)^{-1} = \mathbf{I} - \mathbf{Q} \left(\frac{1}{p_u} \mathbf{I} + \mathbf{Q}^\dagger \mathbf{Q} \right)^{-1} \mathbf{Q}^\dagger. \tag{57}$$

Up to now, we have derived the expected achievable rate under different designs of signature waveform, and the results are summarized in Theorem 1.

REFERENCES

[1] Cisco, "Visual networking index," *Cisco white paper*, 2015.

[2] J. Andrews, S. Buzzi, C. Wan, S. Hanly, A. Lozano, A. Soong, and J. Zhang, "What will 5g be?" *IEEE J. Sel. Areas Commun.*, vol. 32, no. 6, pp. 1065–1082, 2014.

[3] H. Ngo, E. Larsson, and T. Marzetta, "Energy and spectral efficiency of very large multiuser mimo systems," *IEEE Trans. Commun.*, vol. 61, no. 4, pp. 1436–1449, 2013.

[4] T. Marzetta, "Noncooperative cellular wireless with unlimited numbers of base station antennas," *IEEE Trans. Wireless Commun.*, vol. 9, no. 11, pp. 3590–3600, 2010.

[5] F. Boccardi, R. Heath, A. Lozano, T. Marzetta, and P. Popovski, "Five disruptive technology directions for 5g," *IEEE Commun. Mag.*, vol. 52, no. 2, pp. 74–80, 2014.

[6] J. Liu, H. Minn, and A. Gatherer, "The death of 5g part 2: Will analog be the death of massive mimo?" http://http://www.comsoc.org/ctn/death-5g-part-2-will-analog-be-death-massive-mimo, June 2015.

[7] X. Artiga, B. Devillers, and J. Perruisseau-Carrier, "Mutual coupling effects in multi-user massive mimo base stations," *in Proc. IEEE APSURSI*, pp. 1–2, 2012.

[8] C. Masouros, M. Sellathurai, and T. Ratnarajah, "Large-scale mimo transmitters in fixed physical spaces: the effect of transmit correlation and mutual coupling," *IEEE Trans. Commun.*, vol. 61, no. 7, pp. 2794–2804, 2013.

[9] J. Vieira, S. Malkowsky, K. Nieman, Z. Miers, N. Kundargi, L. Liu, I. Wong, V. Owall, O. Edfors, and F. Tufvesson, "A flexible 100-antenna testbed for massive mimo," *in Proc. IEEE GC Wkshps*, pp. 287–293, 2014.

[10] R. Saadane, A. Menouni, R. Knopp, and D. Aboutajdine, "Empirical eigenanalysis of indoor uwb propagation channels," *in Proc. IEEE GLOBECOM*, vol. 5, pp. 3215–3219, 2004.

[11] A. M. Hayar, R. Knopp, and R. Saadane, "Subspace analysis of indoor uwb channels," *EURASIP J. Appl. Signal Process.*, vol. 2005, pp. 287–295, 2005.

[12] Y. Chen, F. Han, Y. Yang, H. Ma, Y. Han, C. Jiang, H. Lai, D. Claffey, Z. Safar, and K. J. R. Liu, "Time-reversal wireless paradigm for green internet of things: an overview," *IEEE Internet Things J.*, vol. 1, no. 1, pp. 81–98, 2014.

[13] A. Inamdar, S. Rylov, A. Talalaevskii, A. Sahu, S. Sarwana, D. Kirichenko, I. Vernik, T. Filippov, and D. Gupta, "Progress in design of improved high dynamic range analog-to-digital converters," *IEEE Trans. Appl. Supercond.*, vol. 19, no. 3, pp. 670–675, 2009.

[14] T. Rappaport, S. Sun, R. Mayzus, H. Zhao, Y. Azar, K. Wang, G. Wong, J. Schulz, M. Samimi, and F. Gutierrez, "Millimeter wave mobile communications for 5g cellular: It will work!" *IEEE Access*, vol. 1, pp. 335–349, 2013.

[15] P. Smulders and L. Correia, "Characterisation of propagation in 60 ghz radio channels," *Electron. Commun. Eng. J.*, vol. 9, no. 2, pp. 73–80, Apr 1997.

[16] F. Han, Y. Yang, B. Wang, Y. Wu, and K. J. R. Liu, "Time-reversal division multiple access over multi-path channels," *IEEE Trans. Commun.*, vol. 60, no. 7, pp. 1953–1965, 2012.

[17] B. P. Bogert, "Demonstration of delay distortion correction by time-reversal techniques," *IRE Trans. Commun. Syst.*, vol. 5, no. 3, pp. 2–7, 1957.

[18] M. Fink and C. Prada, "Acoustic time-reversal mirrors," *Inverse problems*, vol. 17, no. 1, p. R1, 2001.

[19] S. Lehman and A. Devaney, "Transmission mode time-reversal super-resolution imaging," *J. Acoust. Soc. Amer.*, vol. 113, no. 5, pp. 2742–2753, 2003.

[20] D. Liu, G. Kang, L. Li, Y. Chen, S. Vasudevan, W. Joines, Q. Liu, J. Krolik, and L. Carin, "Electromagnetic time-reversal imaging of a target in a cluttered environment," *IEEE Trans. Antennas Propag.*, vol. 53, no. 9, pp. 3508–3066, 2005.

[21] G. Edelmann, T. Akal, W. Hodgkiss, S. Kim, W. Kuperman, and H. Song, "An initial demonstration of underwater acoustic communication using time reversal," *IEEE J. Ocean. Eng.*, vol. 27, no. 3, pp. 602–609, 2002.

[22] A. Derode, P. Roux, and M. Fink, "Robost acoustic time reversal with high order multiple scattering," *Phys. Rev. Lett.*, vol. 75, pp. 4206–4209, 1995.

[23] H. Nguyen, J. Anderson, and G. Pedersen, "The potential of time reversal techniques in multiple element antenna systems," *IEEE Commun. Lett.*, vol. 9, no. 1, pp. 40–42, 2005.

[24] R. de Lacerda Neto, A. Hayar, and M. Debbah, "Channel division multiple access based on high uwb channel temporal resolution," *in Proc. IEEE VTC*, pp. 1–5, 2006.

[25] B. Wang, Y. Wu, F. Han, Y. Yang, and K. J. R. Liu, "Green wireless communications: a time-reversal paradigm," *IEEE J. Select. Areas Commun.*, vol. 29, no. 8, pp. 1698–1710, 2011.

[26] M.-A. Bouzigues, I. Siaud, M. Helard, and A.-M. Ulmer-Moll, "Turn back the clock: time reversal for green radio communications," *IEEE Veh. Technol. Magazine*, vol. 8, no. 1, pp. 49–56, 2013.

[27] R. de Lacerda, L. Cottatellucci, A. Hayar, and M. Debbah, "Asymptotic analysis of channel division multiple access schemes for ultra-wideband systems," *in Proc. IEEE SPAWC*, pp. 186–190, 2008.

[28] R. de Lacerda, A. Hayar, and M. Debbah, "Channel division multiple access: The access solution for uwb networks," *in Proc. IEEE ICUWB*, pp. 309–314, 2014.

[29] Y. Jin, J. Yi, and J. Moura, "Multiple antenna time reversal transmission in ultra-wideband communications," *in Proc. IEEE GlOBECOM*, pp. 26–30, 2007.

[30] Y.-H. Yang, B. Wang, W. S. Lin, and K. J. R. Liu, "Near-optimal waveform design for sum rate optimization in time-reversal multiuser downlink systems," *IEEE Trans. Wireless Commun.*, vol. 12, no. 1, pp. 346–357, 2013.

[31] E. Yoon, S. Kim, and U. Yun, "A time-reversal-based transmission using predistortion for intersymbol interference alignment," *IEEE Trans. Commun.*, vol. 63, no. 2, pp. 455–465, 2014.

[32] Y. Chen, Y.-H. Yang, F. Han, and K. J. R. Liu, "Time-reversal wideband communications," *IEEE Signal Process. Lett.*, vol. 20, no. 12, pp. 1219–1222, 2013.

[33] A. J. Viterbi, *CDMA: principles of spread spectrum communication*. Addison Wesley Longman Publishing Co., Inc., 1995.

[34] I. Azzam and R. Adve, "Linear precoding for multiuser mimo systems with multiple base stations," *in Proc. IEEE ICC*, pp. 1–6, 2009.

[35] L. Kewen, M. Zherui, and H. Ting, "A novel tr-stbc-ofdm scheme for mobile wimax system," *in Proc. IEEE ISAPE*, pp. 1365–1368, 2008.

[36] M. Maaz, M. Helard, P. Mary, and M. Liu, "Performance analysis of time-reversal based precoding schemes in miso-ofdm systems," *in Proc. IEEE VTC*, pp. 1–6, 2015.

[37] A. Pitarokoilis, S. K. Mohammed, and E. G. Larsson, "Uplink performance of time-reversal mrc in massive mimo systems subject to phase noise," *IEEE Trans. Wireless Commun.*, vol. 14, no. 2, pp. 711–723, 2015.

[38] C. Zhou, N. Guo, B. Sadler, and R. Qiu, "Performance study on time reversed impulse mimo for uwb communications based on measured spatial uwb channels," *in Proc. IEEE MILCOM*, pp. 1–6, 2007.

[39] B. Popovic, "Efficient golay correlator," *Electron. Lett.*, vol. 35, no. 17, pp. 1427–1428, Aug 1999.

[40] Z.-H. Wu, Y. Han, Y. Chen, and K. J. R. Liu, "A time-reversal paradigm for indoor positioning system," *IEEE Trans. Veh. Technol.*, vol. 64, no. 4, pp. 1331–1339, 2015.

[41] R. Daniels and R. Heath, "Improving on time-reversal with miso precoding," *in Proc. 8th Int. Symp. Wireless Pers. Commun. Conf.*, pp. 18–22, 2005.

[42] D. Tse and P. Viswanath, "Downlink-uplink duality and effective bandwidths," *in Proc. IEEE ISIT*, 2002.

[43] M. Schubert and H. Boche, "Solution of the multiuser downlink beamforming problem with individual sinr constraints," *IEEE Trans. Veh. Technol.*, vol. 53, no. 1, pp. 18–28, 2004.

[44] R. Hunger and M. Joham, "A general rate duality of the mimo multiple access channel and the mimo broadcast channel," *in Proc. IEEE Global Telecommun. Conf.*, 2008.

[45] E. Telatar, "Capacity of multiple-antenna gaussian channels," *European Trans. Telecommun.*, vol. 10, no. 6, pp. 585–595, 1999.

[46] G. H. Golub and C. F. Van Loan, "Matrix computations," *JHU Press*, vol. 3, 2012.